Modeling Radar Measurement Uncertainty for Look Angle Optimization

Daniel Dowd
HQ Space Operations Command, USSF

ABSTRACT

The purpose of this study is to demonstrate potential operational improvements in the Space Surveillance Network (SSN) characterization of radar measurement uncertainty. This report describes the development of an empirical measurement uncertainty model for a selection of twelve SSN phased array radars. The model is implemented in a look angle optimization algorithm designed to minimize measurement uncertainty across the satellite catalog. A framework is developed to use the model for the improvement of satellite state accuracy and covariance realism.

The SSN performs sensor calibration using independent satellite laser ranging (SLR) precision ephemerides computed for calibration satellites (calsats). Sensor data quality is described in terms of mean offset, standard deviation, and root-mean-square error. These sensor error and uncertainty parameters are captured and implemented in orbit determination and state propagation algorithms. Therefore, the realism of these parameters is fundamental to many critical space domain awareness (SDA) mission areas.

Phased-array radar detections are generally subject to increased uncertainty off boresight due to beam width, effective aperture, and atmospheric effects. Other factors such as phase errors and thermal effects can also contribute to non-uniform uncertainty over a radar's field of view (FOV). Therefore, observation errors and uncertainty can vary significantly with changes in look angle. Capturing this variation accurately would lead to more realistic estimated covariances and improved state accuracies.

Calsat SLR residuals are mapped by their azimuth/elevation coordinates in each radar FOV. A k-nearest neighbor regression algorithm is implemented to estimate the measurement uncertainty at any arbitrary look angle in the FOV. A look angle optimization algorithm is developed and implemented on approximately 1 million observations on 20,000 space objects. For each track, the associated two-line element set (TLE) is propagated and additional look angles are generated over the length of the pass. The measurement uncertainty is calculated at each look angle, and the optimum set of look angles is selected for each pass to minimize the total measurement uncertainty. Trends in both real and optimal look angles are investigated in relation to their relevant measurement uncertainty models. The cumulative reduction in measurement uncertainty for each radar is presented.

The effect of look angle optimization and reduced measurement uncertainty on state accuracy and uncertainty is investigated through the analysis of a representative well-tracked space object. The measurement uncertainty is estimated for each observation along a given track, and each track of the object is split into high and low-uncertainty tracklets. Two datasets of the high and low-uncertainty observations are implemented in a batch differential correction (DC) algorithm, and the improvements in state accuracy and uncertainty of the lower-uncertainty observations is analyzed.

Further analysis is required to demonstrate additional operational impacts of this method of radar uncertainty characterization and look angle optimization. In addition to look angle optimization, the uncertainty model described in this report can be applied to improve uncertainty realism through a "per-observation" error and uncertainty parameter approach to differential correction. A framework is established describing this approach and outlining a methodology for improving rendezvous and proximity operations (RPO) situational awareness (SA) in real-time for space objects of interest.

1. INTRODUCTION

A. What is uncertainty realism?

Covariance realism refers to the accurate description of the uncertainty in the state of a resident space object (RSO) in as much as it can be described as a Gaussian random variable. A *realistic* covariance indicates that the estimated mean and covariance of an RSO accurately reflects its true mean and covariance. Uncertainty realism is a generalized form of covariance realism in that it can describe the effects of nonlinear, non-Gaussian dynamical processes [1].

There are many complex sources of uncertainty that must be considered to accurately characterize the state uncertainty of an RSO [3]:

1. Misrepresentation of the covariance matrix of the input data
2. Missing or incorrect compensation of residual biases of the measurements and misrepresentation of their covariances
3. Missing or incorrect compensation of misassociations
4. Model errors of target state dynamics
5. Algorithm design errors or computational errors
6. Algorithmic uncertainties inherent in inverse problems such as orbit determination and bias estimation
7. Propagation of uncertainty
8. Hardware or software faults

This study focuses on the first two sources of uncertainty and how they might be better characterized by modeling Space Surveillance Network (SSN) radar errors.

B. How is the warfighter dependent on covariance/uncertainty realism?

The most common description of an RSO's uncertainty distribution is the "formal covariance" generated from a least-squares orbit determination process based on uncertainty characteristics of the measurements. These covariance computations are typically "optimistic" in that they overestimate the certainty of an RSO's state and result in a "too-small" covariance. Covariance size, orientation, and shape have outsized impacts on the critical functions of space domain awareness (SDA) that support space control. Relatively small errors in covariance characterization can lead to *orders of magnitude* impacts in probability of collision computation, data association/correlation confidence, and probability of maneuver detection. Optimal sensor management, critical in the data-sparse space domain, is also dependent upon the maintenance of realistic uncertainties. Sensor management algorithms designed to maximize aggregate statistical information gain will tend to provide unnecessary updates to some RSOs and lose others in the presence of unrealistic uncertainties. Developing realistic covariances in support of these mission-critical functions "is perhaps the single most important need if one is to achieve a superior space surveillance capability" [4].

C. How can uncertainty realism be improved?

There is a well-developed body of literature related to the accurate characterization of uncertainty in space surveillance. Astrodynamics force models, algorithmic approaches to the inverse problem, and nonlinear propagation of uncertainty are all areas of research with significant developments over the past couple decades that could improve warfighter SDA and space control. Efforts to implement the developments in these areas must be constrained by the warfighter's requirement to effectively meet today's mission requirements. Therefore, it is worthwhile to investigate the incremental implementation of modern research developments that fit within current operational procedures and doctrine.

This paper will focus on improving the characterization of sensor errors and uncertainties, a topic which has received relatively little attention in the literature but which "may well be the biggest contributor to improved covariance and uncertainty realism" [4]. For objects not experiencing significant drag, the characterization of sensor errors is a key SDA system limitation [2].

D. What is the current operational approach for describing sensor error and uncertainty?

Since the early days of space as a warfighting domain, sensor performance limitations and mission parameters have not required a high-resolution characterization of sensor uncertainty and bias. However, more demanding mission requirements and modern sensor capabilities have exposed previously acceptable approximations as key drivers of error in orbit determination and uncertainty estimation.

Sensor observation modeling is prone to uncertainty and bias as functions of intrinsic sensor measurement variables and can be time-variant in both the short-term (track-to-track) and longer term (hours to days). Phased array radars, dish radars, hybrid radars, and optical tracking systems each have unique sensor level measurement error, processing effects, and calibration procedures that must be considered. Optical data is typically measured with respect to the stellar background in the celestial frame, and has much more accurate angle measurements compared to radar. This study focuses on phased array radar measurement errors and uncertainty.

SSN radar measurements are reported as metric observations of range, azimuth, elevation, and range-rate. The SSN uses satellite laser ranging (SLR) data and precision ephemerides to perform routine sensor calibration for the determination of sensor data quality. Within the calibration process, data quality is represented in mean (bias), standard deviation (sigma), and root-mean-square (RMS) error. If stable, the bias can be subtracted out of the measurements. The standard deviation value represents the uncertainty of the measurements and is used to weight observations in a differential correction and propagation algorithms.

E. How will this study improve sensor error and uncertainty characterization?

This study was initiated with the objective to develop a look angles-based measurement uncertainty model and implement it to correct vector covariance messages (VCMs) using real observations paired with more realistic uncertainty parameters. The expected result of this correction would be improved state accuracies and uncertainties. In the development of the measurement uncertainty model, another area of application presented itself – look angle optimization. Analyzing the look angles of the SSN collects, it is noted that many collects fall in higher-uncertainty areas of the field of view (FOV) – namely, at lower elevations and at the edges of azimuth. Therefore, this study describes two applications of the uncertainty model:

1. Sensor tasking: optimize look angles of collects by minimizing measurement uncertainty across the pass
2. Differential correction (DC): implement more realistic “per-obs” uncertainty parameters in DC algorithms

Optimizing the look angles of collects would lower the measurement uncertainty and therefore reduce satellite state uncertainty across the catalog. Implementing more realistic “per-obs” uncertainty parameters in DC algorithms could improve both satellite state accuracy and uncertainty realism. This study describes the development of a look angles optimization algorithm and presents the improvement in measurement uncertainty for a sample of approximately 1 million real observations on 20,000 space objects. It also establishes a framework for the implementation of more realistic “per-obs” uncertainty parameters in DC and presents initial results.

Once potential improvements in satellite state accuracy and uncertainty are established, the question remains as to how these improvements translate into operational impacts. Conjunction assessment, data or track association/correlation, maneuver detection, and sensor tasking and scheduling are all critical functions of SDA that are fundamentally dependent upon proper and accurate characterization of the uncertainty inherent in the estimation of each space object [4]. The impacts on these types of SDA functions that could be realized through an implementation of this measurement uncertainty model will be investigated in a future study.

2. APPROACH

A. Calibration Satellite Residuals Analysis

This study of sensor error modeling is limited to phased-array radars, which account for the majority of near earth object tracking. These radars have fixed antenna array faces, which subjects their detections to increased uncertainty at the edges of azimuth due to beam width and effective aperture.

SSN sensors are calibrated through the statistical analysis of observation residuals on calsats with high-precision ephemerides. Uncertainty and bias parameters for each phased array radar are calculated for metric observations in range, azimuth, and elevation (RAE). This characterization of measurement uncertainty does not account for uncertainty as a function of track geometry.

Approximately 250,000 observations on 20 calsats across 12 SSN phased array radars are used in the generation of these uncertainty models. Observation residuals in azimuth, elevation, and range are computed with respect to independently determined laser-ranging-generated ephemerides for each calsat. FOV maps are generated, and residuals for azimuth (az) and elevation (el) are plotted according to their az-el coordinates as shown in Figure 1.

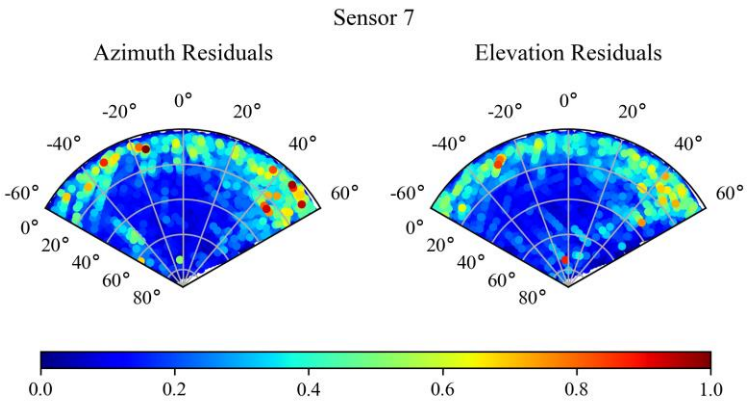

Figure 1: Distributions of Azimuth and Elevation Residuals

Radar angle observations of azimuth and elevation have different uncertainty correlations with look angle. Therefore, each sensor has an uncertainty model for both azimuth and elevation uncertainties. Each of these uncertainty models is weighted differently for each observation according to the instantaneous slope of its corresponding track. For example, if a space object is approaching a sensor head-on, the most relevant uncertainty model would of course be elevation. This reference to the slope of the track is referred to in this report as "in-track measurement uncertainty" for shorthand. In other words, the components of azimuth and elevation which describe the in-track direction of the space object in the az-el space are used to weight each uncertainty model to minimize the measurement uncertainty along that direction. The models describe the in-track direction in terms of azimuth and elevation because range uncertainty tends to be insignificant compared to angular uncertainty for phased array radars. While range uncertainty is not explicitly weighted in the in-track uncertainty model, it tends to be closely correlated with elevation uncertainty.

Each sensor's FOV has been normalized to be north-facing with 120 degrees of azimuth and 90 degrees of elevation. The absolute values of the residuals have been normalized between 0 and 1. The azimuth and elevation residuals are normalized together such that the normalization is consistent for both dimensions. The azimuth and elevation residuals distributions for Sensor 7 are shown in Figure 1. Sensor 7 is used as an example of the uncertainty model throughout this report because it well represents the trends seen across all 12 sensors.

As shown in Figure 1, azimuth and elevation residuals near boresight tend to be much smaller than those at low elevations and at the edges of azimuth. Azimuth and elevation uncertainty maps are generated using these calsat residuals. For each calsat observation, a k-nearest-neighbors algorithm is implemented to compute the standard deviation of the residuals of the 100 nearest adjacent observations. The result is that each individual az-el observation is associated with a standard deviation value at that look angle. The uncertainty maps for sensor 7 are shown in Figure 2.

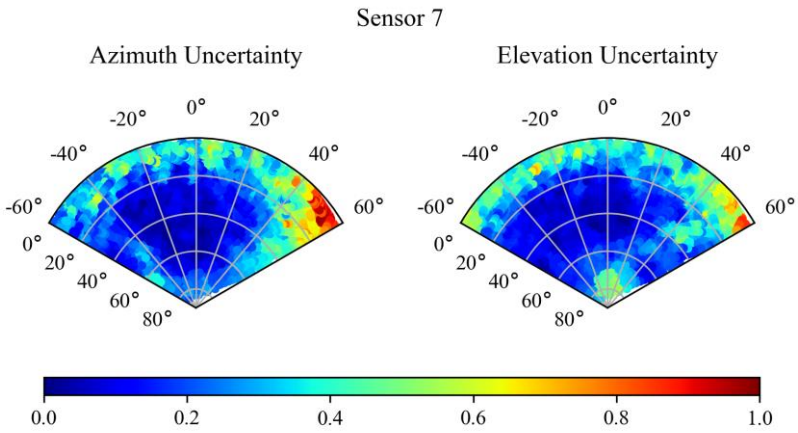

Figure 2: Distributions of Azimuth and Elevation Uncertainty Calculations

These maps highlight the expected uncertainty differences between a measurement taken at low elevation at the edges of azimuth and a measurement taken at boresight.

B. Look Angle Optimization

The expected azimuth and elevation uncertainty for arbitrary FOV look angles is calculated using a regression algorithm on the 5 nearest adjacent standard deviation values weighted by distance. As an arbitrary space object is propagated through the sensor FOV, look angles are generated at 10-second intervals and their expected azimuth and elevation uncertainty values are calculated. The expected in-track measurement uncertainty for each look angle is calculated by weighting the expected az/el uncertainty values according to the az/el slope of the track at that look angle. The expected in-track uncertainty at each look angle of a track across sensor 7 is shown in Figure 3.

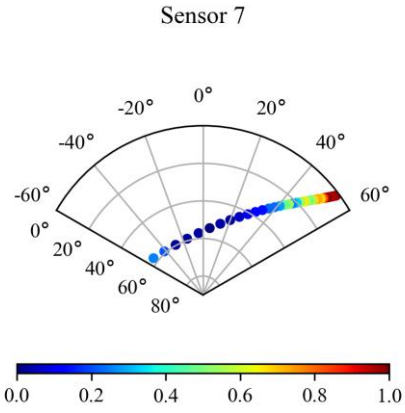

Figure 3: Expected In-Track Uncertainty Across Sensor FOV

As expected from the az/el uncertainty maps, the in-track uncertainty for each look angle tends to be higher at lower elevations and at the edge of azimuth and lower as the track passes near the boresight angle. This approach can be used to minimize in-track measurement uncertainty across the SSN catalog by optimizing the look angles where measurements are taken. For a given set of observations on a space object, the associated TLE is propagated and look angles are generated for the entire pass over the relevant sensor. The in-track measurement uncertainty of the real collects are calculated along with the in-track measurement uncertainty for the rest of the look angles for that pass. The set of consecutive look angles matching the number of real collects is selected to minimize the total in-track measurement uncertainty. An example of this method using the same track from Figure 3 is shown in Figure 4.

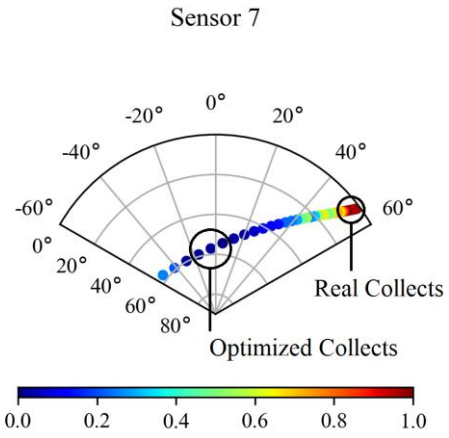

Figure 4: Collects Optimized to Minimize In-Track Uncertainty

The total distribution of real vs optimized measurement look angles and their associated uncertainty values is described in the Results section.

The motivation behind the development of this uncertainty model is to analytically explore the space of sensor uncertainty characterization while remaining close to the warfighter's operational applications. Therefore, there is an emphasis on using real data and accepting some simplifying assumptions to deliver a viable model with immediate potential operational impacts. This model focuses on azimuth and elevation measurement uncertainty as a function of observation look angle. It does not consider other measurement dimensions such as angle rates or range. It is assumed that angle rate uncertainty is well-correlated with angle uncertainty, and range uncertainty is generally much lower than angle uncertainty and therefore less important to minimize. Range uncertainty is also well-correlated with elevation uncertainty. Variations in bias across the FOV are not considered, but this might be a valuable addition to the "per-obs" error and uncertainty parameters application discussed at the end of the Results section. Outlier detection and removal is especially useful when computing parameters which well-approximate measurement uncertainty across the FOV. However, this model describes differences in measurement uncertainty across the FOV by highlighting local regions of higher residuals variance. Therefore, the first implementation of this model as described in this report does not include outlier removal.

Due to the use of the relatively low number of calibration satellites, some sensors have sparse look angles to be used in the regression algorithms to optimize look angles. For the worst examples of sparse models, see sensors 1-3 in the Appendix. This is an open problem – using more calibration data (i.e. a longer period of time) is not ideal because of the temporal nature of measurement uncertainty and routine radar calibrations. Using additional observations on non-calibration objects corrected to post-processed special perturbations (SP) vectors is also not ideal because the resulting residuals are less accurate than residuals calibrated to SLR data. The reduced accuracy of these SP vector-corrected residuals may hide some of the look angle uncertainty correlations foundational to this model. If sensor sites were

incentivized to take calibration measurements across their entire FOVs, it might help alleviate the sparse data problem. Most of the sensors do not suffer from sparse calibration data, and the sensors used in application to differential correction in the Results section are well-characterized.

3. RESULTS

A. Measurement Look Angle Optimization

Approximately 1 million observations on 20,000 space objects across 12 SSN phased array radars are used to evaluate the implementation of the calsat-based uncertainty models to optimize measurement look angles. Figure 5 below contains four charts – the top two are the familiar az/el uncertainty maps for sensor 7 as discussed in the Approach section. The bottom two charts are look angle density maps which highlight the FOV regions with the highest density of collects, both real and optimized. The real collects shown here tend to be most concentrated in the highest-uncertainty area of the FOV – this is characteristic for many of the sensors. The TLE associated with each real set of collects is propagated, and the optimum look angles are selected as illustrated previously in Figure 4.

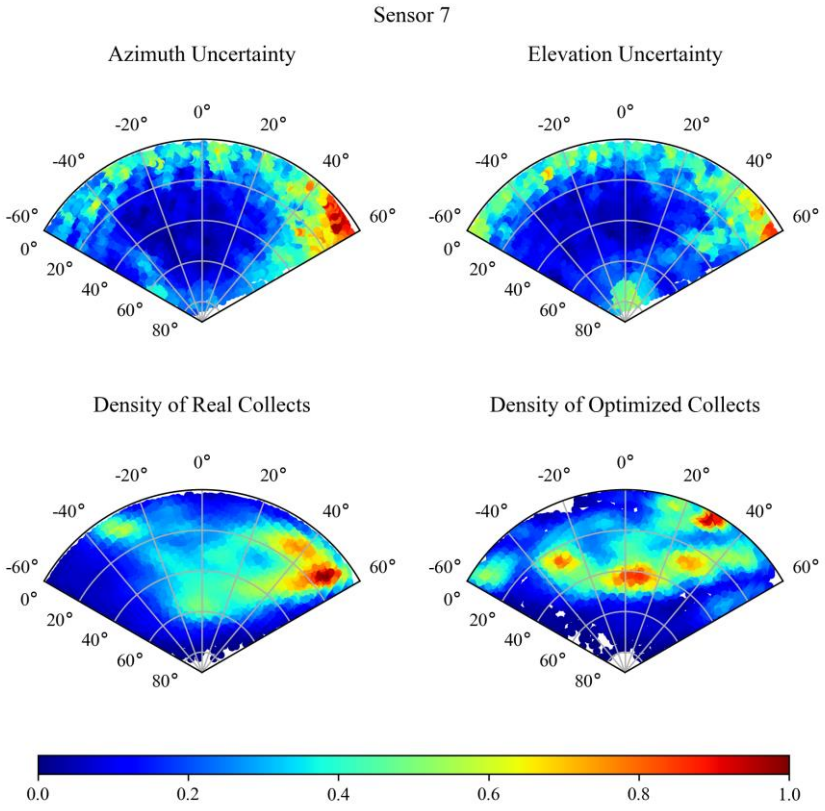

Figure 5: Optimizing Collect Look Angles

The optimized collects tend to be more concentrated close to boresight, as expected. There are other pockets of higher density collect locations driven by relative track geometries across the FOV and local minima in the uncertainty models.

The distribution of normalized in-track uncertainty values associated with the real and optimized collects is shown in Figure 6 below. This figure shows the overall shift towards lower in-track sigma values for the optimized collects.

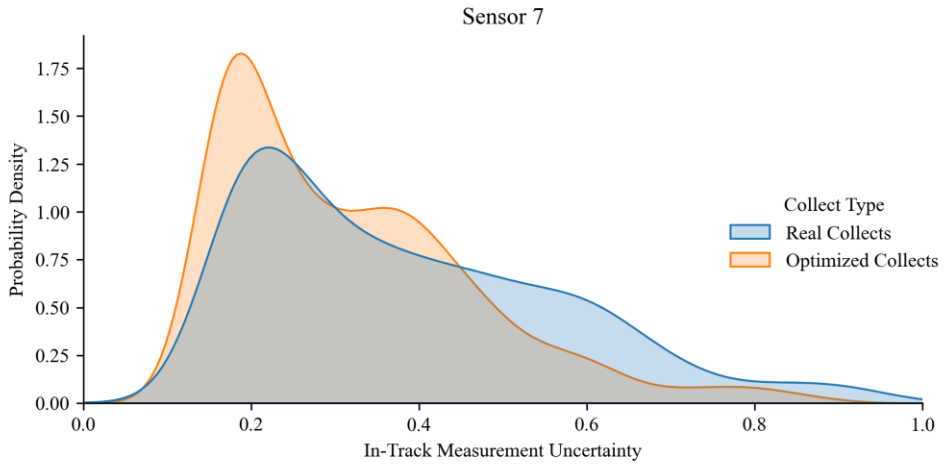

Figure 6: In-Track Uncertainty Distribution

The smooth probability density curves shown in Figure 6 are generated by performing a kernel density estimate over the distribution of in-track sigma values for both real and optimized collects. While there is significant overlap, the real collects are more represented in the upper range of the in-track sigma distribution between 0.5 and 1.0. The optimized collects tend to be more represented over the range of lower sigma values between 0.1 and 0.5.

Another example of look angle optimization and in-track uncertainty reduction is shown for sensor 8 in Figure 7.

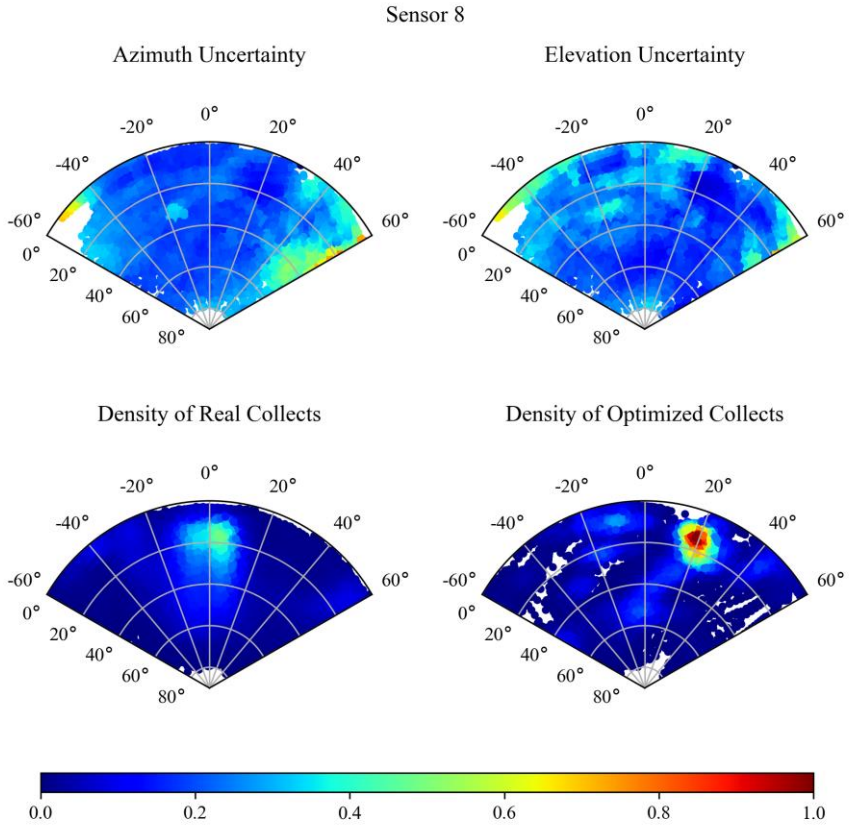

Figure 7: Optimizing Collect Look Angles

The look angle optimization for sensor 8 is interesting because it highlights an advantage of this empirical calsat residuals-based uncertainty model and optimization approach. The real collects captured by sensor 8 are already relatively concentrated close to boresight, and a naïve assumption might be that the resulting uncertainty values might be somewhat optimized. However, after analyzing the uncertainty models, a pocket of low uncertainty can be seen at approximately 20 degrees azimuth and 20 degrees elevation. The optimized look angles show a high density region that perfectly tracks that pocket in the azimuth uncertainty map, indicating many tracks crossing that region geometrically have a high azimuth component to their in-track direction. The in-track uncertainty reduction for sensor 8 is shown in Figure 8

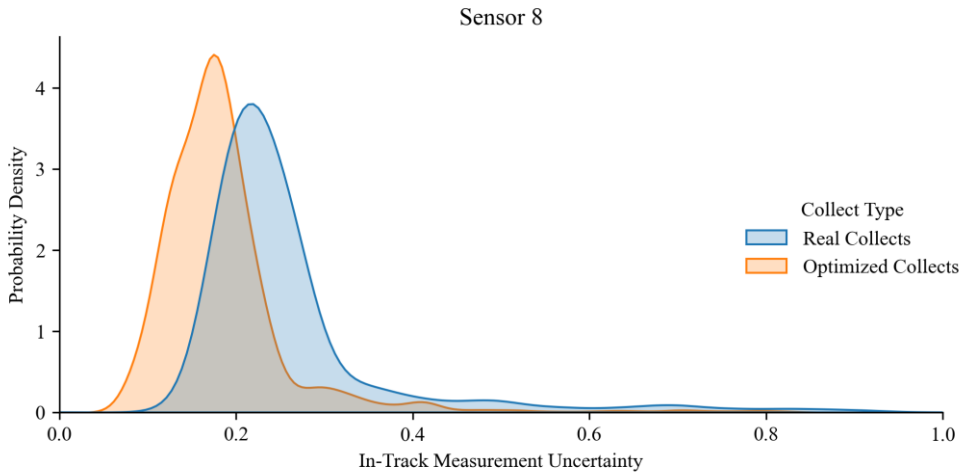

Figure 8: In-Track Uncertainty Distribution

The normalized in-track uncertainty reduction for each sensor is shown in the Appendix.

B. Impact of Look Angle Optimization on RSO State and Uncertainty

The previous section demonstrates the reduction of measurement uncertainty through the optimization of collection look angles. In the context of radar measurements where range uncertainty is typically much better than angle uncertainty, the effect of this az/el uncertainty reduction must be investigated. This section describes the implementation of a batch differential corrections (DC) algorithm to correct an RSO's state and uncertainty using both high-uncertainty and low-uncertainty measurements. The corrected states and uncertainties are compared to "truth" data, and the effect of az/el measurement uncertainty on satellite state accuracy and uncertainty magnitude is analyzed. This analysis is not meant to completely capture the potential statistical impact of look angle optimization on the satellite catalog, but to instead to capture the "order of magnitude" impact of az/el uncertainty reduction in a real-world case study and to serve as a framework for further investigation.

The optimized look angles described in the previous section are generated through propagation, and therefore do not have the uncertainty characteristics of real observations. The optimized look angles could be "noised up" using their associated uncertainty parameters to generate simulated measurements, but this type of noise simulation generally does not capture all of the correlation characteristics of real measurements. To conduct this analysis using real measurements, a well-tracked space object is selected as a case study. This space object is well-tracked across many of the sensors, but particularly so for sensors 4, 6, 7, and 9. These sensors generate long tracks of observations across

their FOVs. The uncertainty models for each sensor are used to estimate the in-track measurement uncertainty for each observation as described in the previous section. The tracks are then split into shorter "high-uncertainty" tracklets and "low-uncertainty" tracklets. These high and low-uncertainty tracklets are representative of "real" and "optimized" collects respectively. A quad-chart for sensor 7 showing an uncertainty model, the full tracks, and the high and low-uncertainty tracklets is shown in Figure 9.

The azimuth uncertainty model for sensor 7 is pictured as a reference, but it should be noted that the in-track uncertainty estimates are computed through a combination of both the azimuth and elevation uncertainty models according to each track's slope across the FOV. As might be expected, the high-uncertainty tracklets are found at low elevations and at the edges of azimuth, and the low-uncertainty tracklets are generally closer to boresight. Each of the tracklets pictured are equal in time and number of observations – due to track geometry relative to the sensor, the tracklets at low elevations appear shorter in length. Some tracklets, notably the highest-uncertainty tracklets at 50-60 degrees azimuth and 10 degrees elevation, appear to be "dropped." That is, they do not have corresponding low-uncertainty tracklets. This phenomenon is an artifact of the observation messages and their track assignments – some tracks may begin on one sensor face and continue across another sensor and thus appear to be "dropped" when looking at individual sensors.

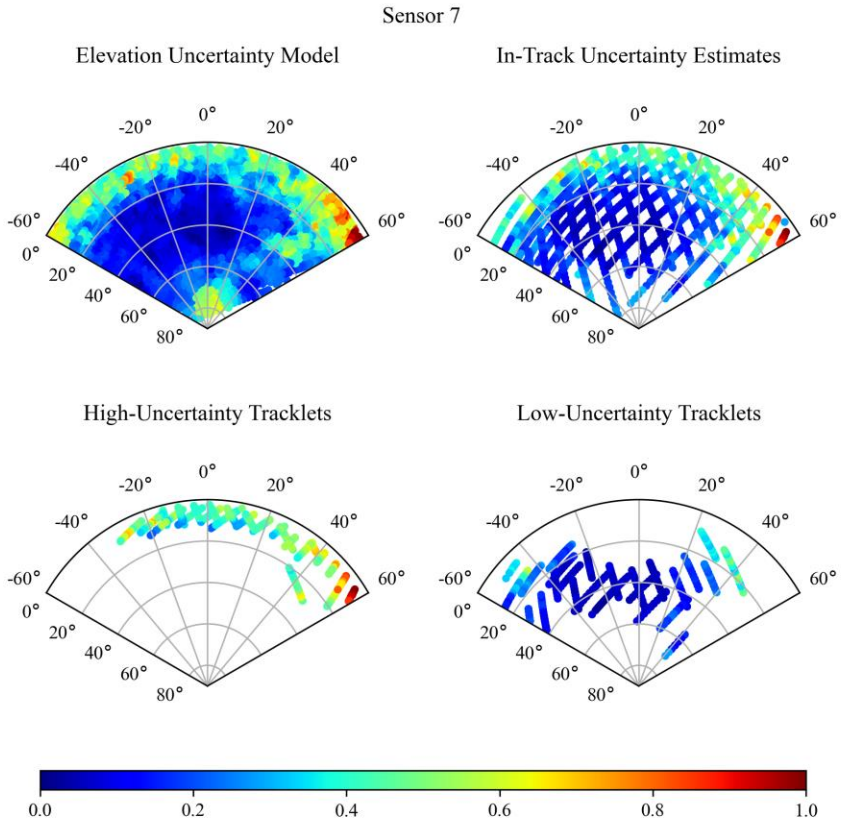

Figure 9: Separating High and Low-Uncertainty Tracklets

The high-uncertainty and low-uncertainty tracklets pictured in Figure 9 are representative of the "real" and "optimized" collection look angles. Another example of separated tracklets for sensor 4 is shown in Figure 10. Sensors

6 and 9 also have long tracks for this object which are similarly split into tracklets and used for DC, and these quad charts are shown in the Appendix.

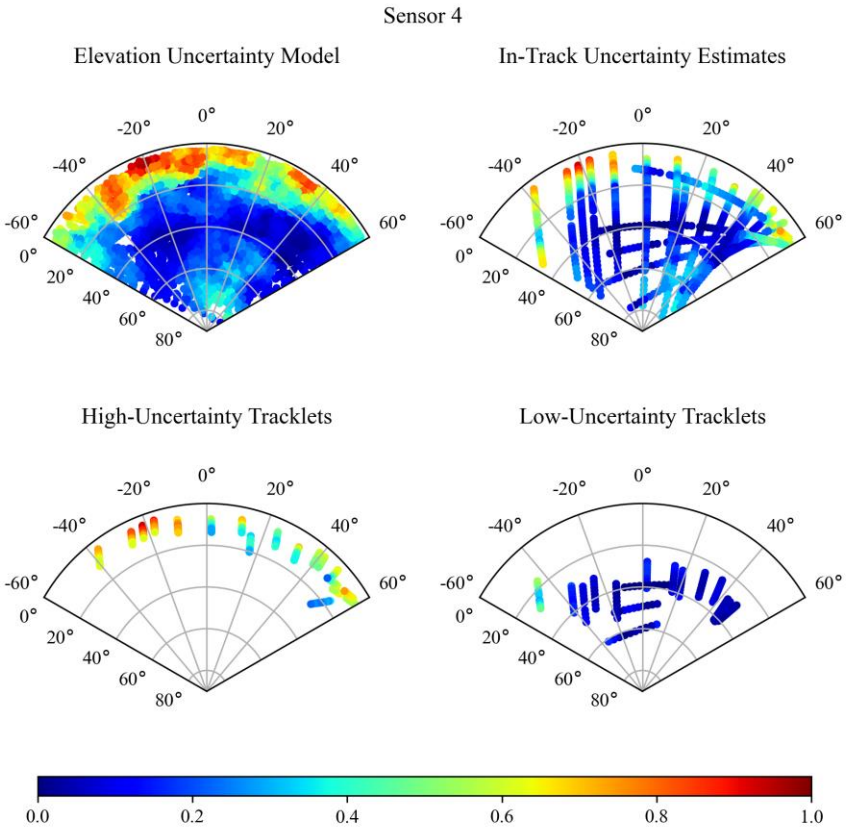

Figure 10: Separating High and Low-Uncertainty Tracklets

The high-uncertainty and low-uncertainty tracklets are implemented in a batch DC algorithm to correct the same initial satellite state and uncertainty to yield two new updated states and uncertainties. By splitting real tracks in this way, the number of external variables that may affect the results is minimized. The two datasets have the same number of measurements taken at similar times of the same object. The only difference is the look angle of each measurement and their respective residuals. The sensor files for each DC are updated to reflect the estimated measurement uncertainty characteristics of each dataset. Each sensor's az/el uncertainty parameters are set to be the mean of the estimated az/el uncertainty parameters for each dataset. For example, the mean of the estimated az/el uncertainty values of the high-uncertainty tracklets for sensor 4 are used to update sensor 4's file for the DC. Thus, for the high-uncertainty tracklet DC, each observation on sensor 4 uses the same high az/el uncertainty values. The use of more realistic "per-obs" uncertainty values is investigated in the next section. The az/el uncertainty values used in the DC of the high-uncertainty tracklets are approximately twice as large as those used in the low-uncertainty tracklet DC.

The two updated states and uncertainties are compared to "truth data" to evaluate their differences. "Truth data" for this case study is the nominal state and uncertainty of the object at the updated time generated from a DC of all measurements taken on all relevant SSN sensors. Because the volume of data is so much larger for the nominal case, it is assumed to be close enough to "truth" for the purpose of comparison with the tracklet DCs.

The relative sizes of the corrected position covariances are shown in Figure 11 below. The low-uncertainty tracklet DC has uncertainty improvements of approximately 70%, 75%, and 80% in the radial, in-track, and cross-track directions respectively. The low-uncertainty tracklet updated state is also 25% more accurate in reference to nominal position "truth" data.

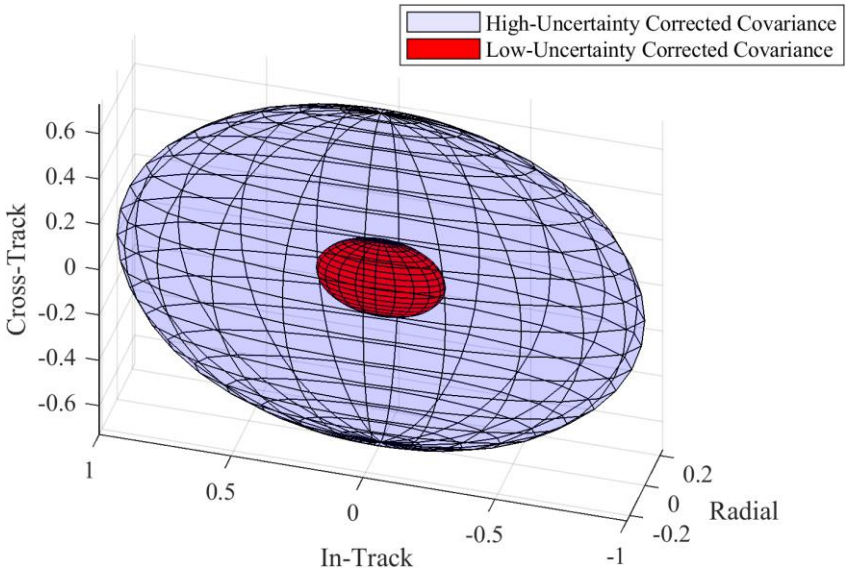

Figure 11: Corrected Position Covariance using High and Low-Uncertainty Tracklets

C. Areas for Further Analysis

The previous sections describe the implementation of the uncertainty models to optimize observation look angles at the sensor level. The uncertainty models can also be leveraged to improve RSO covariance realism by implementing "per-obs" uncertainty and bias parameters in the differential correction algorithms. Instead of weighting each measurement equally across a given pass, a well-tracked object of interest could be corrected using empirically determined, more realistic error and uncertainty parameters both in real-time and in post-processing. This more accurate characterization of the measurement errors and uncertainties would yield to better obs association and situational awareness in rendezvous and proximity operations (RPO) and between closely-spaced objects (CSOs). It would also improve the accuracy of probability of collision calculations. As a starting point for the analysis, observations of a space object will be associated with both a flat sensor file and the look-angle dependent uncertainty models as shown in Figure 12. These two datasets will be implemented in a batch DC algorithm to evaluate the effect of "per-obs" uncertainty parameters on this particular RSO. The expected result would be in the range of that shown in Figure 11 above, but probably a lesser reduction in covariance because there are more observations somewhere in the middle of the uncertainty range.

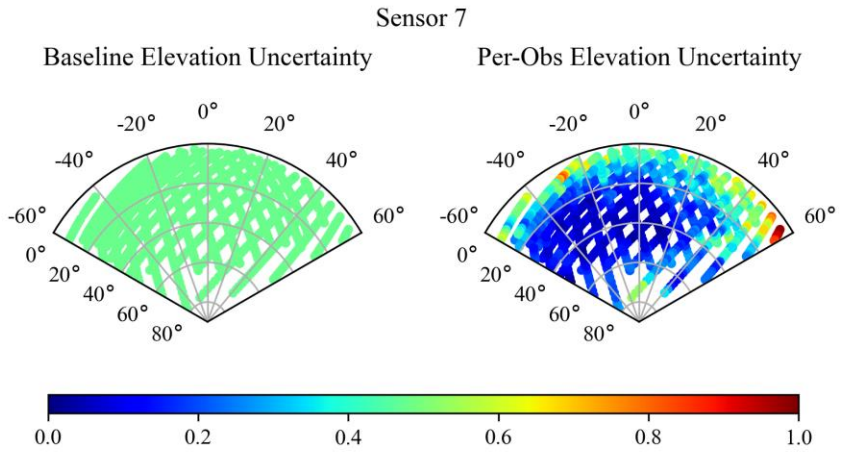

Figure 12: Flat vs Dynamically Assigned Uncertainty Parameters

In addition to objects of interest, this "per-obs" uncertainty approach could feasibly be analyzed across the catalog by comparing nominal states and uncertainties with those obtained by correction with look-angle dependent uncertainty parameters. The analysis of look angle optimization could also be expanded using a wider selection of space objects, sensors, and ranges of uncertainty parameters. Robust simulation data could also be developed to enable better representation of potential improvements across the catalog.

4. CONCLUSION

An empirical measurement uncertainty model has been developed for SSN phased array radars based on calsat residuals as a function of look angle. Two applications of the measurement uncertainty model have been discussed – look angle optimization for accuracy and uncertainty improvement, and a "per-obs" uncertainty consideration for better uncertainty realism. The model has been implemented in a look angle optimization algorithm which yields a reduction in measurement uncertainty across the selection of 12 sensors. The impact of this uncertainty reduction is demonstrated through the implementation of a batch DC algorithm on both low-uncertainty and high-uncertainty tracklets, resulting in approximately 75% reduction in position uncertainty as a result of optimal look angles. The second application of this measurement uncertainty model – a "per-obs" consideration of uncertainty – has been outlined for application both across the satellite catalog and for objects of special interest.

There are several operational impacts driven by one or both of these applications. Conjunction data message (CDM) volume may be reduced dramatically if the state uncertainties across the catalog were improved. Tasking requirements on a constrained network might be reduced – if each observation provides a better update to the state and uncertainty, then fewer observations are required to maintain each object below a certain uncertainty threshold. Conjunction assessment using more realistic uncertainties may result in saved fuel from unnecessary maneuvers and also better collision avoidance. In addition to immediate mission impacts, improving sensor uncertainty characterization in this way may enable many other innovations described in the space surveillance literature – their improvements may otherwise be hidden in rough uncertainty approximations made at the sensor level.

5. REFERENCES

[1] Horwood, J.T.; Aristoff, J.M.; Singh, N.; Poore, A.B.; Hejduk, M.D. Beyond covariance realism: A new metric for uncertainty realism. In Signal and Data Processing of Small Targets 2014; International Society for Optics and Photonics: San Francisco, CA, USA, 2014.

[2] National Research Council, Continuing Kepler's Quest: Assessing Air Force Space Command's Astrodynamics Standards, The National Academies Press, 2012.

[3] Oliver E. Drummond, Terrence L. Ogle, Steven Waugh, "Metrics for evaluating track covariance consistency," Proc. SPIE 6699, Signal and Data Processing of Small Targets 2007, 669916 (13 September 2007); doi: 10.1117/12.740303

[4] Poore, A.B.; Aristoff, J.M.; Horwood, J.T.; Armellin, R.; Cerven, W.T.; Cheng, Y.; Cox, C.M.; Erwin, R.S.; Frisbee, J.H.; Hejduk, M.D.; et al. Covariance and Uncertainty Realism in Space Surveillance and Tracking; Numerica Corporation Fort Collins United States: Fort Collins, CO, USA, 2016.

6. APPENDIX